Syntheses, Crystal Structures, and Properties of New Layered Alkali-Metal Molybdenum(VI) Methylphosphonates: $Cs_2(MoO_3)_3PO_3CH_3$ and $Rb_2(MoO_3)_3PO_3CH_3$

William T. A. Harrison,† Laurie L. Dussack, and Allan J. Jacobson*

Department of Chemistry, University of Houston, Houston, Texas 77204-5641

Received May 3, 1995[⊗]

The hydrothermal syntheses and crystal structures of two new alkali-metal molybdenum(VI) methylphosphonates, $Cs_2(MoO_3)_3PO_3CH_3$ and $Rb_2(MoO_3)_3PO_3CH_3$, are described. These isostructural phases are built up from hexagonal tungsten oxide like layers of vertex-sharing MoO_6 octahedra, capped on one side by P–CH_3 entities (as $[PO_3CH_3]^{2-}$ methylphosphonate groups). Interlayer Cs^+ or Rb^+ cations provide charge balance for the anionic sheets. The MoO_6 octahedra display a distinctive three short + three long Mo–O bond distance distribution within the MoO_6 unit. Powder X-ray, infrared, Raman, and thermogravimetric data for $Cs_2(MoO_3)_3PO_3CH_3$ are also presented. The structures of $Cs_2(MoO_3)_3PO_3CH_3$ and $Rb_2(MoO_3)_3PO_3CH_3$ are related to those of the recently reported $M_2(MoO_3)_3SeO_3$ (M = NH_4, Cs) materials but show a three-layer repeating motif, rather that the two-layer repeat found in the $M_2(MoO_3)_3SeO_3$ structures. This different layer repeat pattern may be correlated with the steric effect of the methylphosphonate group. Crystal data: $Cs_2(MoO_3)_3PO_3CH_3$, trigonal, $R\bar{3}$ (No. 146), a = 7.304(2) Å, c = 20.02(1) Å, V = 924.7 Å^3, Z = 3; $Rb_2(MoO_3)_3PO_3CH_3$, trigonal, $R\bar{3}$ (No. 146), a = 7.307(2) Å, c = 20.040(4) Å, V = 926.7 Å^3, Z = 3.

Introduction

We recently reported the syntheses and structures of new layered materials based on the hexagonal tungsten oxide (HTO) motif (Figure 1) of corner-sharing octahedra. $NH_4(VO_2)_3(SeO_3)_2$[1] and $K(VO_2)_3(SeO_3)_2$[2] are the first layered-HTO type phases containing vanadium (V^V) as the octahedral cation. In these two phases, both sides of the infinite vanadium/oxygen layers are capped by selenium atoms (as pyramidal $[SeO_3]^{2-}$ selenite groups). Isostructural $(NH_4)_2(MoO_3)_3SeO_3$ and $Cs_2(MoO_3)_3SeO_3$[3] contain similar vertex-linked MoO_6 layers (Mo^{VI}) but are only capped by Se atoms on one side of the molybdenum/oxygen sheets. Related double-capped layered materials described earlier include synthetic potassium antimony phosphate/arsenate hydrates[4] and various sulfate minerals.[5]

This new family of layered HTO-type phases is notable for the unusual octahedral metal coordination environments found in these materials. In $NH_4(VO_2)_3(SeO_3)_2$,[1] the vanadium(V) atom is displaced from the geometric center of its six oxygen atom neighbors toward an octahedral *edge*, resulting in a two short + two medium + two long V–O bond length distribution within the VO_6 unit. The more common V^VO_6 distortion mode observed in phases such as $VOPO_4$[6] involves the vanadium atom shifting along a V–O bond. This leads to one short "vanadyl" V=O bond, four intermediate-length V–O links, and one long V–O bond. Conversely, in $(NH_4)_2(MoO_3)_3SeO_3$ and $Cs_2(MoO_3)_3SeO_3$,[3] the molybdenum atom is locally displaced toward an octahedral *face*, resulting in a three short + three long Mo–O bond distance distribution within the MoO_6 unit. The commoner MoO_6 distortion mode (Mo atom shifts toward an octahedral edge) leads to two short Mo=O bonds in *cis* configuration, two intermediate Mo–O links, and two long Mo–O bonds.[7]

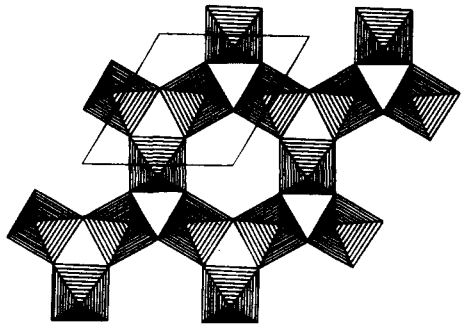

Figure 1. STRUPLO polyhedral view of a generic hexagonal tungsten oxide (HTO) octahedral layer, viewed down the crystallographic [001] direction, showing the infinite network of octahedral three- and six-rings.

Because of the unusual anisotropy of the layers present in these structures, we are currently investigating the synthesis of related compounds with other "capping groups." In previous work, we have shown that similar structures may be formed by phases which contain $[SeO_3]^{2-}$ and $[PO_3CH_3]^{2-}$ units. For example, the compounds $VOSeO_3 \cdot H_2O$[8] and $VO(PO_3CH_3) \cdot 1.5H_2O$[9] have very similar layer structures.

In this paper we report the syntheses, structures, and some properties of the isostructural, singly-capped, HTO-based layered materials $Cs_2(MoO_3)_3PO_3CH_3$ and $Rb_2(MoO_3)_3PO_3CH_3$.

Experimental Section

Syntheses. $Cs_2(MoO_3)_3PO_3CH_3$ was hydrothermally prepared from 0.56 g of $CsOH \cdot H_2O$ (3.33 mmol of Cs), 0.60 g of MoO_3 (4.17 mmol of Mo), 0.136 g of 98% $CH_3PO_3H_2$ (1.39 mmol of P), and 6 mL of

† Current address: Department of Chemistry, University of Western Australia, Nedlands, WA 6907, Australia.

⊗ Abstract published in *Advance ACS Abstracts,* August 1, 1995.

(1) Vaughey, J. T.; Harrison, W. T. A.; Dussack, L. L.; Jacobson, A. J. *Inorg. Chem.* **1994**, *33*, 4370.
(2) Harrison, W. T. A.; Dussack, L. L.; Jacobson, A. J. *Acta Crystallogr.*, in press.
(3) Harrison, W. T. A.; Dussack, L. L.; Jacobson, A. J. *Inorg. Chem.* **1994**, *33*, 6043.
(4) Tournoux, M.; Ganne, M.; Piffard, Y. *J. Solid State Chem.* **1992**, *96*, 141.
(5) Wang, R.; Bradley, W. F.; Steinfink, H. *Acta Crystallogr.* **1965**, *18*, 249.
(6) Jordan, B.; Calvo, C. *Can. J. Chem.* **1973**, *51*, 2621.
(7) Kilhborg, L. *Ark. Kemi* **1963**, *21*, 357.
(8) Huan, G.; Johnson, J. W.; Brady, J. F.; Goshorn, D. P.; Jacobson, A. J. *Mater. Chem. Phys.* **1993**, *35*, 199.
(9) Huan, G.; Johnson, J. W.; Jacobson, A. J.; Goshorn, D. P.; Merola, J. S. *Chem. Mater.* **1991**, *3*, 539.

0020-1669/95/1334-4774$09.00/0

Table 1. X-ray Powder Data for $Cs_2(MoO_3)_3PO_3CH_3$

hkl	d_{obs} (Å)	d_{calc} (Å)	I_{rel}[a]
003	6.680	6.680	77
101	6.032	6.032	24
012	5.348	5.349	11
104	3.928	3.927	9
110	3.650	3.652	28
015	3.385	3.386	48
006	3.337	3.340	100
113	3.204	3.204	100
021	3.123	3.124	33
202	3.015	3.016	60
024	2.674	2.674	13
107	2.608	2.608	37
205	2.483	2.483	4
116	2.646	2.465	11
211	2.374	2.374	7
212	2.326	2.326	11
009	2.227	2.227	17
214	2.158	2.158	6
027	2.123	2.122	9
125	2.053	2.053	12
303	2.011	2.011	29

[a] $100 \times I/I_{max}$.

H_2O (molar ratio Cs:Mo:PO_3CH_3 = ~2.4:3:1). These reactants were sealed in a 23-mL Teflon-lined Parr bomb and heated to 180 °C for 48 h. The pH of the final filtrate was 5.6. The overall yield of solid product, based on Mo, was ~80%. Bluish-green, brilliantly faceted rhombohedrally-shaped crystals of $Cs_2(MoO_3)_3PO_3CH_3$ (maximum size ~0.5 mm) were recovered by vacuum filtration followed by recovery on an 80-mesh sieve. The fines passing through the 180-μm openings contained the title compound plus a secondary phase of unidentified bright yellow powder. Pure $Cs_2(MoO_3)_3PO_3CH_3$ material was hand-sorted for the physical measurements described below.

$Rb_2(MoO_3)_3PO_3CH_3$ was hydrothermally prepared from 0.57 g of 50% aqueous RbOH solution (2.78 mmol of Rb), 0.60 g of MoO_3 (4.17 mmol of Mo), 0.136 g of 98% $CH_3PO_3H_2$ (1.39 mmol of P), and 6 mL of H_2O (molar ratio Rb:Mo:PO_3CH_3 = 2:3:1) using a procedure similar to that used for the $Cs_2(MoO_3)_3PO_3CH_3$ synthesis. The filtrate pH was 4.6. The yield of bluish rhombs of $Rb_2(MoO_3)_3PO_3CH_3$ was only ~2%, and the reaction is not repeatable. Variation of reaction conditions (starting pH, concentrations, temperature) did not result in increased yields of $Rb_2(MoO_3)_3PO_3CH_3$ but led to solutions or powders of unknown composition.

X-ray Powder Data. Diffraction data for a crushed sampled of $Cs_2(MoO_3)_3PO_3CH_3$ were recorded on a Scintag XDS 2000 automated powder diffractometer (Cu Kα radiation, $\bar{\lambda}$ = 1.541 78 Å, T = 25(2) °C). Autoindexing indicated a rhombohedral phase with a = 7.3037(5) Å and c = 20.040(2) Å (V = 925.8 Å^3). The indexed powder data for $Cs_2(MoO_3)_3PO_3CH_3$ are listed in Table 1. The amount of $Rb_2(MoO_3)_3PO_3CH_3$ available was insufficient to perform powder measurements.

Crystal Structure Determinations. The crystal structure of $Cs_2(MoO_3)_3PO_3CH_3$ was determined by single-crystal X-ray methods: A brilliantly faceted, slightly translucent, bluish rhomb (dimensions ~0.3 × 0.2 × 0.2 mm) was mounted on a thin glass fiber with cyanoacrylate glue, and room-temperature [25(2) °C] intensity data were collected on an Enraf-Nonius CAD4 automated four-circle diffractometer (graphite-monochromated Mo Kα radiation, λ = 0.710 73 Å). Preliminary measurements indicated a rhombohedrally-centered lattice (Table 2), in agreement with the X-ray powder data.

A total of 1082 intensity data were collected for $2\theta \leq 70°$. During data reduction, an absorption correction based on ψ scans (minimum 3.34, maximum 4.45) was applied to the data. The systematic absence condition ($-h + k + l \neq 3n$) indicated space groups $R3$, $R\bar{3}$, $R32$, $R3m$, and $R\bar{3}m$. Initial data merges indicated that Laue class $\bar{3}$ was probably the correct one [R_{Int} = 3.09%, 909 merged data, 906 data with $I > 3\sigma(I)$].

The crystal structure model of $Cs_2(MoO_3)_3PO_3CH_3$ was developed in space group $R3$, with initial heavy-atom positions (Cs, Mo, P) located by using the direct-methods program SHELXS-86.[10] No reasonable starting configuration could be established in the other possible space groups, and $R3$ was assumed for the remainder of the crystallographic analysis. $R3$ is the only space group of these possibilities which allows for the presence of singly-capped octahedral layers (*vide infra*). The oxygen and carbon atom positions were located from Fourier difference maps during the refinement (program: CRYSTALS[11]). The hydrogen atom was located geometrically, assuming that the H atoms of the CH_3 group were staggered with respect to the O atoms of the PO_3 moiety, and the H atom positional parameters were refined by riding on the carbon atoms. The final cycles of full-matrix least-squares refinement were against F and included anisotropic temperature factors and a Larson-type secondary extinction correction.[12] Complex, neutral-atom scattering factors were obtained from ref 13. Crystallographic data for $Cs_2(MoO_3)_3PO_3CH_3$ are summarized in Table 2.

Table 2. Crystallographic Parameters

	$Cs_2(MoO_3)_3PO_3CH_3$	$Rb_2(MoO_3)_3PO_3CH_3$
empirical formula	$Cs_2Mo_3PO_{12}CH_3$	$Rb_2Mo_3PO_{12}CH_3$
a (Å)	7.304(2)	7.307(2)
c (Å)	20.02(1)	20.040(4)
V (Å^3)	924.7	926.7
Z	3	3
fw	791.63	696.76
space group	$R3$ (No. 146)	$R3$ (No. 146)
T (°C)	25(2)	25(2)
λ(Mo Kα) (Å)	0.710 73	0.710 73
ϱ_{calc} (g/cm^3)	4.26	3.75
μ(Mo Kα) (cm^{-1})	89.0	107.3
$R(F)$[a] (%)	2.92	4.91
$R_w(F)$[b] (%)	3.94[c]	4.94[d]

[a] $R = 100 \times \sum||F_o| - |F_c||/\sum|F_o|$. [b] $R_w = 100 \times [\sum w(|F_o| - |F_c|)^2/\sum w|F_o|^2]^{1/2}$. [c] $w_i = 1/\sigma(F_i)^2$. [d] w_i described by a three-term Chebychev polynomial.

The structure of $Rb_2(MoO_3)_3PO_3CH_3$ was established in similar fashion: A slightly-translucent rhomb, dimensions ~0.35 × 0.25 × 0.25 mm, was mounted on a thin glass rod with cyanoacrylate glue, and room-temperature [25(2) °C] intensity data were collected on an Enraf-Nonius CAD4 diffractometer as above. Intensity data (2θ < 70°, 3074 peaks scanned) were collected as before: R_{Int} = 2.98%, 912 observable data with $I > 3\sigma(I)$. Absorption (minimum 2.62, maximum 2.94) was accounted for on the basis of ψ scans. The structure of $Rb_2(MoO_3)_3PO_3CH_3$ was refined in space group $R3$ using the $Cs_2(MoO_3)_3PO_3CH_3$ final atomic coordinates as a starting model (Rb substituting for Cs). Crystallographic data for $Rb_2(MoO_3)_3PO_3CH_3$ are listed in Table 2.

Thermogravimetric Analysis. TGA data for $Cs_2(MoO_3)_3PO_3CH_3$ were collected on a DuPont 9900 instrument (ramp 5 °C/min under flowing N_2 gas). Heating to 400 °C resulted in no weight loss, and powder X-ray measurements on the TGA residue showed that $Cs_2(MoO_3)_3PO_3CH_3$ had maintained its structure at this temperature. Further heating to 600 °C under nitrogen resulted in a two-step weight loss at ~480 °C (3.8%) and ~550 °C (3.4%). X-ray measurements on the post-TGA residue indicated poorly crystalline MoO_2 together with glassy materials.

A TGA run under an oxygen atmosphere to 600 °C showed decomposition at 475 °C, followed by a gradual weight gain to 575 °C. The yellow, glassy residue is amorphous.

Spectroscopic Data. Infrared spectra (KBr pellet method) for $Cs_2(MoO_3)_3PO_3CH_3$ and $Rb_2(MoO_3)_3PO_3CH_3$ were measured from 400 to 4000 cm^{-1} on a Galaxy FTIR 5000 series spectrometer. Raman data (KBr pellet) for $Cs_2(MoO_3)_3PO_3CH_3$ were obtained using a coherent K-2 Kr^+ ion laser excited at 406.7 nm. Counts were accumulated at 1-s intervals for every wavenumber over the range 100–1700 cm^{-1} (Spex 1403 double monochromator/Hamamatsu 928 photomultiplier detection system).

(10) Sheldrick, G. M. *SHELXS-86 User Guide*; Crystallography Department, University of Göttingen: Göttingen, Germany, 1986.
(11) Watkin, D. J.; Carruthers, J. R.; Betteridge, P. W. *CRYSTALS User Guide*; Chemical Crystallography Laboratory; Oxford University: Oxford, U.K., 1993.
(12) Larson, A. C. *Acta Crystallogr.* **1967**, *23*, 664.
(13) Cromer, D. T. *International Tables for X-Ray Crystallography*; Kynoch Press: Birmingham, U.K., 1974; Vol. IV; Table 2.3.1.

Table 3. Atomic Positional/Thermal Parameters for $Cs_2(MoO_3)_3PO_3CH_3$

atom	*x*	*y*	*z*	U_{eq}[a]
Cs(1)	0	0	0.17280(6)	0.0240
Cs(2)	1/3	2/3	0.23065(5)	0.0150
Mo(1)	0.00836(9)	0.54101(9)	0.06017(5)	0.0068
P(1)	−1/3	1/3	0.1869(2)	0.0084
O(1)	0.077(1)	0.542(1)	−0.0209(3)	0.0127
O(2)	0.2166(9)	0.7965(8)	0.0902(3)	0.0080
O(3)	−0.2132(9)	0.580(1)	0.0519(3)	0.0094
O(4)	−0.102(1)	0.451(1)	0.1629(3)	0.0120
C(1)	−1/3	1/3	0.2764(7)	0.0122
H(1)[b]	−0.4748	0.2614	0.2922	0.02[c]

[a] U_{eq} (Å^2) = $(U_1U_2U_3)^{1/3}$. [b] H atom refined by riding on C(1). [c] U_{iso} (Å^2) (not refined).

Table 4. Bond Distances (Å)/Angles (deg) for $Cs_2(MoO_3)_3PO_3CH_3$

Cs(1)−O(1) × 3	3.230(6)	Cs(1)−O(2) × 3	3.130(6)
Cs(2)−O(1) × 3	3.071(7)	Cs(2)−O(2) × 3	3.215(6)
Cs(2)−O(3) × 3	3.467(6)	Cs(2)−O(4) × 3	3.070(7)
Mo(1)−O(1)	1.698(7)	Mo(1)−O(2)	1.822(5)
Mo(1)−O(2)	2.105(6)	Mo(1)−O(3)	1.788(6)
Mo(1)−O(3)	2.113(6)	Mo(1)−O(4)	2.186(6)
P(1)−O(4) × 3	1.540(6)	P(1)−C(1)	1.79(2)
C(1)−H(1)	0.95		
O(1)−Mo(1)−O(2)	102.5(3)	O(1)−Mo(1)−O(2)	90.7(3)
O(2)−Mo(1)−O(2)	86.7(3)	O(1)−Mo(1)−O(3)	101.7(3)
O(2)−Mo(1)−O(3)	103.0(3)	O(2)−Mo(1)−O(3)	162.1(2)
O(1)−Mo(1)−O(3)	88.9(3)	O(2)−Mo(1)−O(3)	162.3(3)
O(2)−Mo(1)−O(3)	79.7(2)	O(3)−Mo(1)−O(3)	87.5(4)
O(1)−Mo(1)−O(4)	164.5(3)	O(2)−Mo(1)−O(4)	89.5(3)
O(2)−Mo(1)−O(4)	80.2(2)	O(3)−Mo(1)−O(4)	84.8(3)
O(3)−Mo(1)−O(4)	77.2(2)	O(4)−P(1)−O(4)	110.7(3)
O(4)−P(1)−C(1)	108.2(3)	Mo(1)−O(2)−Mo(1)	132.1(3)
Mo(1)−O(3)−Mo(1)	150.4(3)	Mo(1)−O(4)−P(1)	126.8(4)

Table 5. Atomic Positional/Thermal Parameters for $Rb_2(MoO_3)_3PO_3CH_3$

atom	*x*	*y*	*z*	U_{eq}[a]
Rb(1)	0	0	0.17421(8)	0.0140
Rb(2)	1/3	2/3	0.23203(7)	0.0052
Mo(1)	0.0080(1)	0.5409(1)	0.06118(6)	0.0116
P(1)	−1/3	1/3	0.1872(2)	0.0124
O(1)	0.078(1)	0.543(1)	−0.0197(4)	0.0182
O(2)	0.216(1)	0.795(1)	0.0912(3)	0.0138
O(3)	−0.212(1)	0.582(1)	0.0521(4)	0.0157
O(4)	−0.102(1)	0.454(1)	0.1636(4)	0.0182
C(1)	−1/3	1/3	0.2772(8)	0.0163
H(1)[b]	−0.4748	0.2614	0.2916	0.02[c]

[a] U_{eq} (Å^2) = $(U_1U_2U_3)^{1/3}$. [b] H atom refined by riding on C(1). [c] U_{iso} (Å^2) (not refined).

Results

Crystal Structures. Final atomic positional and equivalent isotropic thermal parameters for $Cs_2(MoO_3)_3PO_3CH_3$ are listed in Table 3, with selected bond distance/angle data in Table 4. Comparable data for $Rb_2(MoO_3)_3PO_3CH_3$ are listed in Tables 5 and 6.

$Cs_2(MoO_3)_3PO_3CH_3$ and $Rb_2(MoO_3)_3PO_3CH_3$ are isostructural new phases built up from cesium/rubidium ions and layers of vertex-sharing MoO_6 and O_3P-CH_3 units, which are connected by Mo−O−Mo′ and Mo−O−P bonds. A detail of the Mo/P/O/CH_3 layer is shown in Figure 2, and the complete crystal structure is illustrated in Figure 3. Assuming full occupancy of all the atomic sites for these phases ensures charge neutrality, and models involving both cation and anion vacancies were not considered further.

As with the phases mentioned in the Introduction, $Cs_2(MoO_3)_3PO_3CH_3$ and $Rb_2(MoO_3)_3PO_3CH_3$ are built up from hexagonal

Table 6. Bond Distances (Å)/Angles (deg) for $Rb_2(MoO_3)_3PO_3CH_3$

Rb(1)−O(1) × 3	3.226(8)	Rb(1)−O(2) × 3	3.142(7)
Rb(2)−O(1) × 3	3.076(8)	Rb(2)−O(2) × 3	3.222(8)
Rb(2)−O(3) × 3	3.452(8)	Rb(2)−O(4) × 3	3.080(8)
Mo(1)−O(1)	1.699(8)	Mo(1)−O(2)	1.817(7)
Mo(1)−O(2)	2.111(7)	Mo(1)−O(3)	1.786(7)
Mo(1)−O(3)	2.119(7)	Mo(1)−O(4)	2.180(8)
P(1)−O(4) × 3	1.537(8)	P(1)−C(1)	1.80(2)
C(1)−H(1)	0.94		
O(1)−Mo(1)−O(2)	102.2(3)	O(1)−Mo(1)−O(2)	90.6(3)
O(2)−Mo(1)−O(2)	86.2(4)	O(1)−Mo(1)−O(3)	101.2(4)
O(2)−Mo(1)−O(3)	103.1(3)	O(2)−Mo(1)−O(3)	162.9(3)
O(1)−Mo(1)−O(3)	88.7(4)	O(2)−Mo(1)−O(3)	162.4(3)
O(2)−Mo(1)−O(3)	79.9(3)	O(3)−Mo(1)−O(3)	88.0(4)
O(1)−Mo(1)−O(4)	165.4(4)	O(2)−Mo(1)−O(4)	89.1(3)
O(2)−Mo(1)−O(4)	80.9(3)	O(3)−Mo(1)−O(4)	84.9(3)
O(3)−Mo(1)−O(4)	78.2(3)	O(4)−P(1)−O(4)	111.0(3)
O(4)−P(1)−C(1)	107.9(3)	Mo(1)−O(2)−Mo(1)	132.5(4)
Mo(1)−O(3)−Mo(1)	149.6(4)	Mo(1)−O(4)−P(1)	126.7(5)

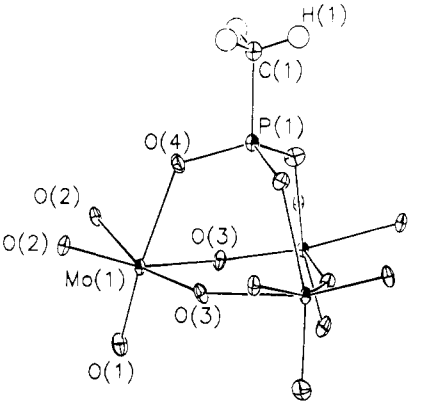

Figure 2. ORTEP view of the Mo/O/P/CH_3 building unit of $Cs_2(MoO_3)_3PO_3CH_3$, showing the atom-labeling scheme (50% thermal ellipsoids).

tungsten oxide[14] type layers of corner-sharing MoO_6 units. Each MoO_6 unit shares four of its Mo−O vertices with similar neighbors, with these Mo−O−Mo′ bonds roughly aligned in the *ab* plane. The two remaining apical Mo−O bonds point approximately in the *c* direction, one above the plane and one below. Three-rings and six-rings of octahedra result from this arrangement (Figure 1). The three apical oxygen atoms of the three-rings on one side of the octahedral layer are capped by P−CH_3 units (*i.e.* methylphosphonate $[PO_3CH_3]^{2-}$ groups), thus forming Mo−O−P bonds. The overall sheet stoichiometry is $[(MoO_3)_3PO_3CH_3]^{2-}$, with charge compensation provided by two crystallographically distinct interlayer cesium or rubidium cations.

In both $Cs_2(MoO_3)_3PO_3CH_3$ and $Rb_2(MoO_3)_3PO_3CH_3$, the MoO_6 octahedron is significantly distorted from octahedral regularity. The molybdenum atom (site symmetry 1) makes a short "molybdyl" bond to O(1), which is not bound to any other atom (d = 1.698(7) Å for the Cs phase; d = 1.699(8) Å for the Rb phase). Two bonds each to O(2) and O(3) form the four in-sheet links to neighboring Mo atoms. For both phases, the two distinct inter Mo atom links [*via* O(2) and O(3)] both contain a short (<1.85 Å) and a long (>2.10 Å) Mo−O bond, *i.e.* Mo=O−Mo′ and Mo−O=Mo′ links. The final Mo−O vertex, O(4), is the bridge between P and Mo. Thus, each molybdenum atom has three short Mo−O bonds (d < 1.85 Å), each of which is *trans* to a long (d > 2.10 Å) Mo−O bond. This distortion may be viewed as a displacement of the molybdenum atom from the center of the MoO_6 octahedron

(14) Gérand, B.; Nowogrocki, G.; Guenot, J.; Figlarz, M. *J. Solid State Chem.* **1979**, *29*, 429.

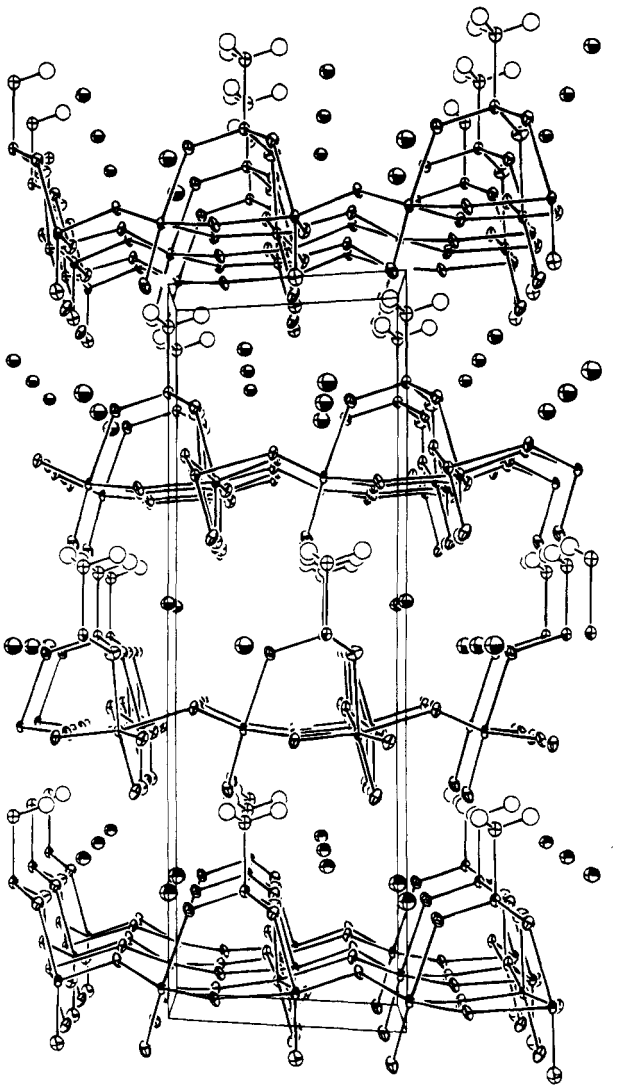

Figure 3. Unit-cell packing of $Cs_2(MoO_3)_3PO_3CH_3$, viewed down [010], showing the sheet structure (Cs−O contacts not shown).

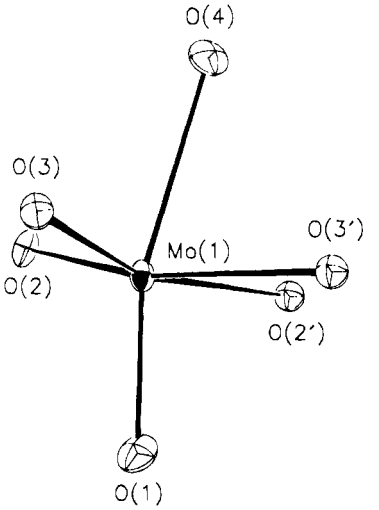

Figure 4. Detail of the MoO_6 octahedron in the $Cs_2(MoO_3)_3PO_3CH_3$ structure, showing the local Mo atom displacement toward the octahedral face defined by atoms O(1), O(2), and O(3).

toward an octahedral face (Figure 4) and was also observed for the Mo atoms in the structures of $(NH_4)_2(MoO_3)_3SeO_3$ and $Cs_2(MoO_3)_3SeO_3$.[2] The magnitudes of these displacements from the centroid of the six oxygen atoms are similar for both $Cs_2(MoO_3)_3PO_3CH_3$ (0.342 Å) and $Rb_2(MoO_3)_3PO_3CH_3$ (0.335 Å). This MoO_6 distortion is unusual, but Brese−O'Keeffe bond valence sum (BVS) calculations are typical for Mo^{VI} in both cases (BVS[Mo(1)] = 6.03 for the cesium phase; BVS[Mo(1)] = 6.03 for the rubidium phase).

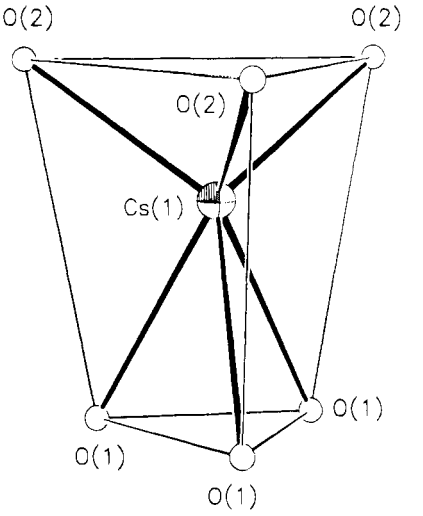

Figure 5. Cs(1) coordination in $Cs_2(MoO_3)_3PO_3CH_3$. Nonbonding O···O contacts are indicated by thin lines.

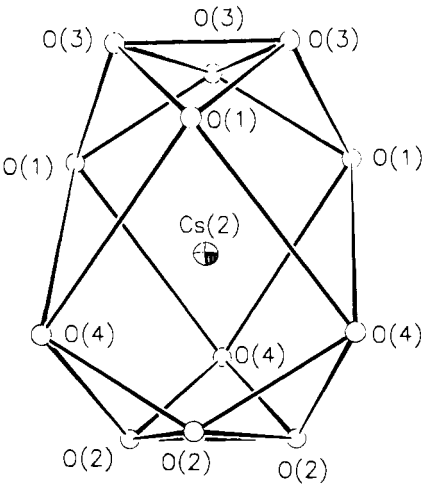

Figure 6. Cs(2) coordination in $Cs_2(MoO_3)_3PO_3CH_3$.

The methylphosphonate group has typical geometrical parameters in both $Cs_2(MoO_3)_3PO_3CH_3$ and $Rb_2(MoO_3)_3PO_3CH_3$ (Tables 4 and 6). The P and C atoms are on a 3-fold axis, and three equivalent P(1)−O(4) bonds result, each of which bridges to a different MoO_6 unit. The hydrogen atoms attached to the sp^3 carbon atom were geometrically placed (*vide supra*) and have a minimum separation of approximately 3 Å from nearby nonbonding oxygen atoms. In both structures, the four distinct oxygen atoms partake in Mo−O−Mo′ bridges [O(2) and O(3)], an Mo−O(4)−P link, and a terminal Mo−O(1) bond.

The two crystallographically-distinct cation sites (both with site symmetry 3) are both found in the interlayer region for these phases. Cs(1) and Rb(1) are six-coordinate (Figure 5) to nearby oxygen atoms and form distorted trigonal prisms. Cs(2) and Rb(2) are 12-coordinate (Figure 6) and form six bonds to oxygen atoms in the each of the two adjacent $(MoO_3)_3PO_3CH_3$ sheets. Bond valence sums for these cations are as follows: BVS[Cs(1)] = 0.78, BVS[Cs(2)] = 1.56, BVS[Rb(1)] = 0.50, BVS[Rb(2)] = 1.00 (expected value = 1.00 in all cases). Thus, the $M(2)$ species appears to be more strongly bonded into the $M_2(MoO_3)_3PO_3CH_3$ structure for both the Cs and Rb phases. We note that the thermal factor of Cs(1) is larger than that of Cs(2), and the same situation applies for the

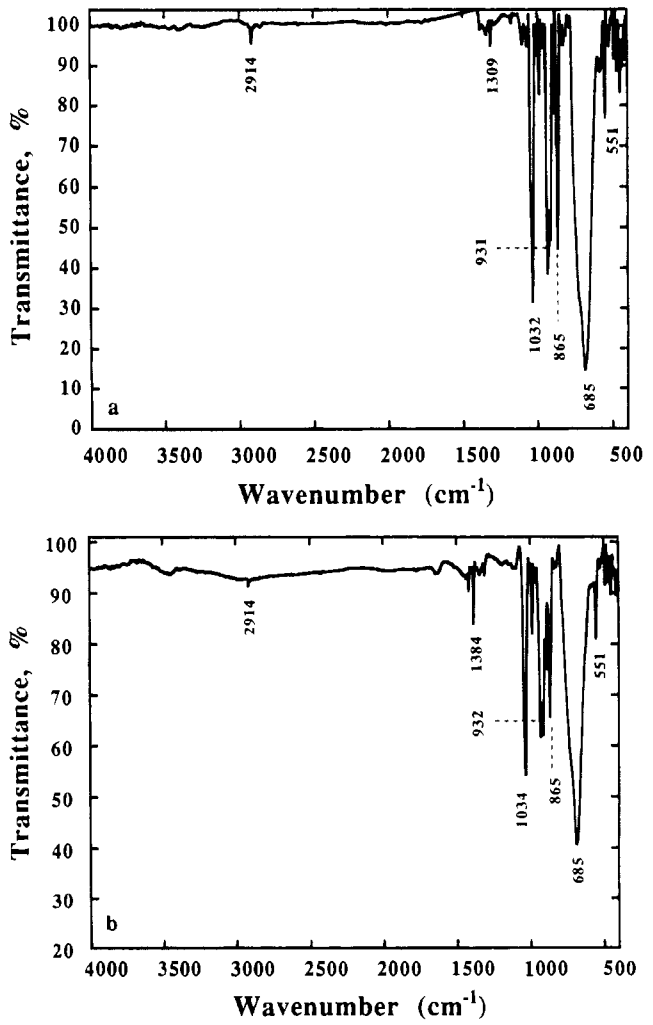

Figure 7. IR spectra of (a) $Cs_2(MoO_3)_3PO_3CH_3$ and (b) $Rb_2(MoO_3)_3PO_3CH_3$.

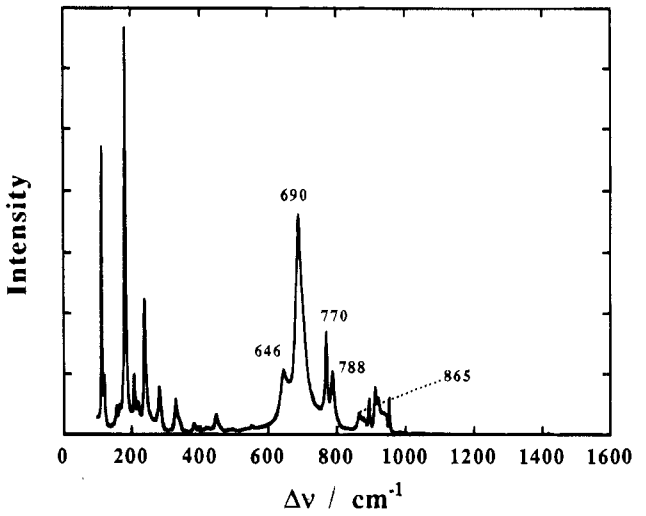

Figure 8. Raman spectrum of $Cs_2(MoO_3)_3PO_3CH_3$.

Rb(1)/Rb(2) cations. These BVS values suggest that the stability of this structure type is not crucially determined by the bonding requirements of the guest cations. However, these species must have some role to play in stabilizing the HTO-type six-ring windows and must be large enough to bridge adjacent $(MoO_3)_3PO_3CH_3$ layers. We are doing further work to elucidate the stability limits of this structure type with cation size.

Spectroscopy. The infrared and Raman spectra of $Cs_2(MoO_3)_3PO_3CH_3$ are shown in Figures 7a and 8, respectively. Bands in the IR spectrum at 2914 and 1309 cm^{-1} represent C–H stretching and bending modes associated with the CH_3 group on the methylphosphonate entity. The sharp peak at 865 cm^{-1} represents an asymmetric MoO_6 mode, corresponding to the very weak feature observed in the Raman spectrum at 865 cm^{-1}. The strong, broad band at 685 cm^{-1} (IR) is a MoO_6 symmetric stretching mode and corresponds to the strong, broad feature at 690 cm^{-1} in the Raman spectrum. Peaks at 1034 and 932 cm^{-1} (IR) and at 788 and 770 cm^{-1} (Raman) correspond to various P–O modes. Figure 7b shows the IR spectrum of $Rb_2(MoO_3)_3PO_3CH_3$, which corresponds closely to that of $Cs_2(MoO_3)_3PO_3CH_3$.

Discussion

$Cs_2(MoO_3)_3PO_3CH_3$ and $Rb_2(MoO_3)_3PO_3CH_3$ are new phases, based on a layered hexagonal tungsten oxide motif of vertex-linked $Mo^{VI}O_6$ octahedra, singly-capped by PCH_3 entities. Hydrothermal synthesis was successful in producing single crystals of both $Cs_2(MoO_3)_3PO_3CH_3$ and $Rb_2(MoO_3)_3PO_3CH_3$, but the overall yield for the $Rb_2(MoO_3)_3PO_3CH_3$ was low and unknown impurity phases also resulted. The reason for the poor yield for the Rb phase is unknown. Although the starting reaction mixture was stoichiometric with respect to the intended $Rb_2(MoO_3)_3PO_3CH_3$ product, the resulting physical conditions (especially pH) for the hydrothermal process may result in the trapping of other metastable phases.

The crystal structures of $Cs_2(MoO_3)_3PO_3CH_3$ and $Rb_2(MoO_3)_3PO_3CH_3$ may be contrasted with those of the related $(NH_4)_2(MoO_3)_3SeO_3$ and $Cs_2(MoO_3)_3SeO_3$.[2] In $Cs_2(MoO_3)_3PO_3CH_3$ and $Rb_2(MoO_3)_3PO_3CH_3$, the molybdenum–oxygen layers are singly-capped by P–CH_3 entities, whereas in $(NH_4)_2(MoO_3)_3SeO_3$ and $Cs_2(MoO_3)_3SeO_3$ the capping is done by selenium atoms. All four of these phases show a similar, unusual MoO_6 distortion, in which the Mo atom is displaced from the center of its octahedron of oxygen atom neighbors toward an octahedral face, resulting in a three short + three long Mo–O bond distance distribution within the MoO_6 unit. The magnitudes of the displacements (0.33 Å for $(NH_4)_2(MoO_3)_3SeO_3$; 0.30 Å for $Cs_2(MoO_3)_3SeO_3$; 0.34 Å for $Cs_2(MoO_3)_3PO_3CH_3$; 0.34 Å for $Rb_2(MoO_3)_3PO_3CH_3$) are similar for all four phases. The displacement of a Mo^{VI} d^0 cation in octahedral coordination may be understood in terms of a second-order Jahn–Teller effect:[15] The small, highly-charged Mo^{VI} species lowers the energy of its unoccupied 4d orbitals, and these are then able to interact strongly with the filled p orbitals of the oxygen atom species, resulting in several closely-spaced molecular orbitals. "Spontaneous" distortion of the MoO_6 unit will remove degeneracies in these energy levels. The magnitude and *direction* of the cation displacement inside the octahedron are much harder to predict from first principles and may reflect a combination of second-order electronic effects, lattice stresses, and cation–cation repulsions, as discussed recently by Kunz and Brown.[16]

A significant difference between the $M_2(MoO_3)_3PO_3CH_3$ and $M_2(MoO_3)_3SeO_3$ phases may be seen by comparing the spatial relationship between adjacent HTO layers in the crystallographic *c* directions. In the $M_2(MoO_3)_3SeO_3$ phases, a two-layer repeat (*ABAB*...) motif is seen, whereas in $M_2(MoO_3)_3PO_3CH_3$, a three-layer (*ABCABC*...) periodicity is observed. In both the $M_2(MoO_3)_3PO_3CH_3$ and $M_2(MoO_3)_3SeO_3$ phases, the layers are displaced in the hexagonal *a* and *b* directions with respect to their neighbors. This layer-staggering effect means that there

(15) Burdett, J. K. *Molecular Shapes*; Wiley-Interscience: New York, 1980.
(16) Kunz, M.; Brown, I. D. *J. Solid State Chem.* **1995**, *115*, 395.

are no pseudoinfinite six-ring channels in the $M_2(MoO_3)_3PO_3CH_3$ or $M_2(MoO_3)_3SeO_3$ topologies, comparable to the infinite six-ring channels seen in the hexagonal WO_3 structure.[14] For comparison, the double-capped phases $NH_4(VO_2)_3(SeO_3)_2$[1] and $K(VO_2)_3(SeO_3)_2$[2] adopt a two-layer (*ABAB*...) repeat pattern, while the $K_3(SbO_2)_3(XO_4)_2$ phases (X = P, As)[4] adopt a three-layer (*ABCABC*...) repeat pattern. The numbers of interlayer cations [one for $NH_4(VO_2)_3(SeO_3)_2$ and $K(VO_2)_3(SeO_3)_2$; two for the $M_2(MoO_3)_3PO_3CH_3$ and $M_2(MoO_3)_3SeO_3$ structure types; three for $K_3(SbO_2)_3(XO_4)_2$)] make direct comparison among these three structure types difficult.

The different stacking patterns for the $M_2(MoO_3)_3SeO_3$ and $M_2(MoO_3)_3PO_3CH_3$ phases are manifested in the different unit cell lengths observed for these phases [$a(M_2(MoO_3)_3SeO_3) \approx a(M_2(MoO_3)_3PO_3CH_3)$; $c(M_2(MoO_3)_3SeO_3) \approx {}^2/_3\, c(M_2(MoO_3)_3PO_3CH_3)$]. The three-layer motif of the $M_2(MoO_3)_3PO_3CH_3$ phases may be rationalized in terms of the steric requirements of the methylphosphonate group. In the $M_2(MoO_3)_3PO_3CH_3$ phases, every $P-CH_3$ group points toward a six-ring window in the next $(MoO_3)_3PO_3CH_3$ layer. The layer separation (interlayer Mo−Mo distance) for $Cs_2(MoO_3)_3PO_3CH_3$ is 6.67 Å, with a comparable value of 6.68 Å for $Rb_2(MoO_3)_3PO_3CH_3$. This suggests that the cation has little role in defining the interlayer separation in these phases, which is largely determined by the steric requirements of the methylphosphonate group.

Conversely, in the $M_2(MoO_3)_3SeO_3$ structures, the selenium atom points toward a three-ring (uncapped) in the adjacent $(MoO_3)_3SeO_3$ layer. The layer separations for $(NH_4)_2(MoO_3)_3SeO_3$ (6.02 Å) and for $Cs_2(MoO_3)_3SeO_3$ (6.19 Å) suggest that the cation plays more of a structural role in defining the layer separation in these phases. However, the role of H-bonding, if any, in $(NH_4)_2(MoO_3)_3SeO_3$ is unknown at present.

Acknowledgment. We thank Paul Meloni and Roman Czernuszewicz for assistance in collecting the Raman data. This work was funded by the National Science Foundation (Grant DMR9214804) and the Robert A. Welch Foundation (Grant E-1207).

Supporting Information Available: Tables of anisotropic thermal factors for $Cs_2(MoO_3)_3PO_3CH_3$ and $Rb_2(MoO_3)_3PO_3CH_3$ (1 page). Ordering information is given on any current masthead page.

IC950533M